Atmospheric
Chemistry
and Physics

Open Access

Influence of crustal dust and sea spray supermicron particle concentrations and acidity on inorganic NO_3^- aerosol during the 2013 Southern Oxidant and Aerosol Study

H. M. Allen[1,a], D. C. Draper[1,b], B. R. Ayres[1], A. Ault[2,3], A. Bondy[2], S. Takahama[4], R. L. Modini[4], K. Baumann[5], E. Edgerton[5], C. Knote[6], A. Laskin[7], B. Wang[7], and J. L. Fry[1]

[1]Department of Chemistry, Reed College, Portland, OR, USA
[2]Department of Chemistry, University of Michigan, Ann Arbor, MI, USA
[3]Department of Environmental Health Sciences, University of Michigan, Ann Arbor, MI, USA
[4]Ècole Polytechnique Fèdèrale de Lausanne, Lausanne, Switzerland
[5]Atmospheric Research & Analysis, Inc., Cary, NC, USA
[6]Meteorologisches Institut, Ludwig-Maximilians-Universität, Munich, Germany
[7]William R. Wiley Environmental Molecular Sciences Laboratory, Pacific Northwest National Laboratory, Richland, WA, USA
[a]now at: Division of Chemistry and Chemical Engineering, California Institute of Technology, Pasadena, CA, USA
[b]now at: Department of Chemistry, University of California, Irvine, CA, USA

Correspondence to: J. L. Fry (fry@reed.edu)

Abstract. Inorganic aerosol composition was measured in the southeastern United States, a region that exhibits high aerosol mass loading during the summer, as part of the 2013 Southern Oxidant and Aerosol Study (SOAS) campaign. Measurements using a Monitor for AeRosols and GAses (MARGA) revealed two periods of high aerosol nitrate (NO_3^-) concentrations during the campaign. These periods of high nitrate were correlated with increased concentrations of supermicron crustal and sea spray aerosol species, particularly Na^+ and Ca^{2+}, and with a shift towards aerosol with larger (1 to 2.5 μm) diameters. We suggest this nitrate aerosol forms by multiphase reactions of HNO_3 and particles, reactions that are facilitated by transport of crustal dust and sea spray aerosol from a source within the United States. The observed high aerosol acidity prevents the formation of NH_4NO_3, the inorganic nitrogen species often dominant in fine-mode aerosol at higher pH. Calculation of the rate of the heterogeneous uptake of HNO_3 on mineral aerosol supports the conclusion that aerosol NO_3^- is produced primarily by this process, and is likely limited by the availability of mineral cation-containing aerosol surface area. Modeling of NO_3^- and HNO_3 by thermodynamic equilibrium models (ISORROPIA II and E-AIM) reveals the importance of including mineral cations in the southeastern United States to accurately balance ion species and predict gas–aerosol phase partitioning.

1 Introduction

Aerosol optical thickness measurements using remote sensing techniques indicate a high concentration of aerosol in the atmosphere over the southeastern United States during the summer months (Portmann et al., 2009). These aerosols likely arise from the significant concentrations of regional inorganic pollutants such as sulfur dioxide, and from the oxidation of high concentrations of biogenic volatile organic compounds emitted from regional vegetation (Goldstein et al., 2009). Anthropogenic NO_x (i.e., NO and NO_2) acts as an important precursor in the oxidation of biogenic volatile organic compounds that leads to aerosol formation. Global emissions of NO_x and other anthropogenic nitrogen compounds have

increased tenfold in the last century and are expected to become one of the most prevalent pollutants in the near future as SO_2 concentrations decrease (Bauer et al., 2007; Doering et al., 2011). Although NO_x concentrations are gradually decreasing in the southeastern United States due to improved emission control technology (Russell et al., 2012). Thus, characterization of NO_x emissions and their relationship to aerosol formation can provide valuable constraints for atmospheric scientists and regulatory agencies seeking to understand the production of aerosol in the southeastern United States.

Aerosol NO_3^- forms in the atmosphere when NO_x, emitted from high-temperature combustion processes in vehicle engines and industrial facilities, reacts with OH radicals to form HNO_3 (Seinfeld and Pandis, 2006). This reaction is considered the dominant sink of daytime NO_x. Nighttime oxidation of NO_2 may form HNO_3 via a N_2O_5 intermediate (Jacob, 1999). After formation, HNO_3 dissociates in water droplets to produce aerosol NO_3^-. In the southeastern United States, NO_3^- typically comprises between 0.5 and $2\,\mu g\,m^{-3}$ of the annual $13–18\,\mu g\,m^{-3}$ total non-water aerosol mass (Blanchard and Hidy, 2003; Bauer et al., 2007). Yet HNO_3 is a semi-volatile species, and will readily partition between the gas and aerosol phases. As a result, the thermodynamic relationships governing aerosol NO_3^- concentrations are complex and highly dependent on the aerosol's chemical composition, the ambient temperature, and the aerosol water content. Furthermore, aqueous-phase reactions may recycle HNO_3 back to the gas phase, further complicating the partitioning (Wang and Laskin, 2014).
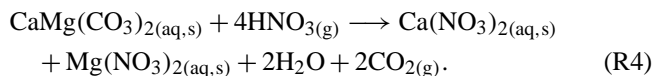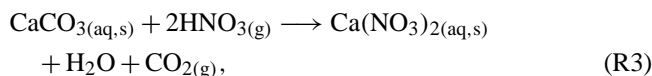
The anthropogenically emitted gas phase species NO_x, NH_3, and SO_2 serve as precursors for the formation of inorganic aqueous aerosol containing NO_3^-, NH_4^+, and SO_4^{2-}. In this multiphase system, the presence of aqueous NH_4^+ and SO_4^{2-} indirectly influences the phase partitioning of HNO_3 due to effects on aerosol hygroscopicity, liquid water content, and acidity. In general, aqueous NH_4^+ will associate with NO_3^- and SO_4^{2-} to produce, respectively, fine mode ($<1\,\mu m$ diameter) NH_4NO_3 and various forms of ammoniated sulfates such as $(NH_4)_2SO_4$, $(NH_4)_3H(SO_4)_2$, and NH_4HSO_4, which are considered the dominant forms of these ions in the atmosphere (Finlayson-Pitts and Pitts, 2000; Seinfeld and Pandis, 2006; Baker and Scheff, 2007). However, the formation of NH_4NO_3 is typically limited by the amount of NH_4^+ available to balance both SO_4^{2-} and NO_3^- (Blanchard et al., 2000). Addition of acidic H_2SO_4 to the aerosol system, as occurs in environments dominated by SO_2 pollution, will drive NH_3 condensation into and HNO_3 evaporation from the particles as the aerosol system reestablishes a new thermodynamic equilibrium. The NH_3 driven into the particle phase will associate with sulfate, leaving HNO_3 in the gas phase (Stelson and Seinfeld, 1982):

$$2NH_4NO_{3(aq,s)} \underset{-H_2SO_4}{\overset{+H_2SO_4}{\rightleftharpoons}} (NH_4)_2SO_4 + 2HNO_{3(g)} \tag{R1}$$
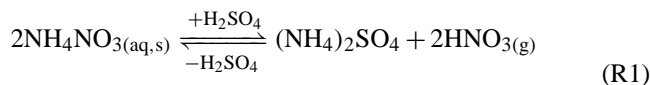
Under acidic conditions (e.g., high concentrations of SO_4^{2-}), nitrate aerosol may still be formed when HNO_3 undergoes heterogeneous chemistry on the reactive surfaces of supermicron ($>1\,\mu m$ diameter) aerosol, such as sea spray and crustal dust, which act as reactive sinks for HNO_3 (Dentener et al., 1996; Zhuang et al., 1999; Underwood et al., 2001; Yeatman et al., 2001; Lee et al., 2008). In sea salt (primarily NaCl) aerosol, HNO_3 displaces the Cl^- ion to form $NaNO_3$ and gas phase HCl, resulting in aerosol chloride depletion (Brimblecombe and Clegg, 1988; Zhuang et al., 1999):

$$NaCl_{(aq,s)} + HNO_{3(g)} \longrightarrow NaNO_{3(aq,s)} + HCl_{(g)}. \tag{R2}$$
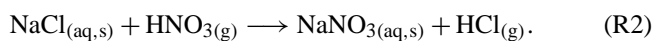
The multicomponent nature of sea spray means that analogous reactions may occur with other sea salt species, such as $MgCl_2$. Similarly, HNO_3 reacts with carbonates in crustal dust, such as $CaCO_3$ and $CaMg(CO_3)_2$, to form $Ca(NO_3)_2$ and $Mg(NO_3)_2$ (Laskin et al., 2005a; Gibson et al., 2006):

$$CaCO_{3(aq,s)} + 2HNO_{3(g)} \longrightarrow Ca(NO_3)_{2(aq,s)}$$
$$+ H_2O + CO_{2(g)}, \tag{R3}$$
$$CaMg(CO_3)_{2(aq,s)} + 4HNO_{3(g)} \longrightarrow Ca(NO_3)_{2(aq,s)}$$
$$+ Mg(NO_3)_{2(aq,s)} + 2H_2O + 2CO_{2(g)}. \tag{R4}$$

Sea spray and crustal dust have important implications for the total nitrogen budget, as these reactions facilitate a shift of NO_3^- from the fine mode to the coarse mode ($>2.5\,\mu m$ diameter), and can enhance the amount of nitrate present in the aerosol. Globally, greater than 40 % of the total nitrate concentration is associated with crustal dust (Usher et al., 2003). Models of HNO_3 reactions on sea spray aerosols with diameters in the $1–3\,\mu m$ range show that the equilibrium partitioning times are reached on the order of approximately 5 to 20 h (Meng and Seinfeld, 1996; Erickson et al., 1999; Fridlind and Jacobson, 2000), shorter than the dry-deposition time of nitric acid in the air. As a result of these moderate equilibration times compared with the relatively shorter lived supermicron particles in marine air, the uptake of HNO_3 by marine aerosol decreases the atmospheric lifetime and associated transport of total NO_3^- relative to HNO_3 (Kane et al., 1994). The effect of crustal dust on the lifetime and transport of total NO_3^- differs from that of marine aerosol due to the typically lower mass-weighted dry-deposition velocities and fluxes and to the lofting and transport of dust above the planetary boundary layer (Arimoto et al., 1997). Inclusion of mineral species in global models increases the tropospheric nitrate aerosol burden by 44 %, with coarse-mode nitrate increasing by around 53 % depending upon the chemical composition of the emitted crustal dust (Karydis et al., 2015).

The present study seeks to understand the conditions under which inorganic nitrate aerosol formation occurs in the

atmosphere in the southeastern United States. Measurements of inorganic aerosol and gas phase species were collected using ion chromatography, in an area of rural Alabama influenced by both biogenic and anthropogenic emissions. These measurements, coupled with air mass back trajectory analysis for source elucidation and with thermodynamic modeling, provide an insight into the fate of NO_x emissions and the formation of nitrate aerosol under conditions in which NH_4NO_3 formation is unfavored.

2 Experimental

2.1 Site description

The Southern Oxidant and Aerosol Study (SOAS) field campaign took place from 1 June to 15 July 2013 as part of a multi-institutional effort to understand biosphere–atmosphere interactions in the southeastern United States. The site chosen for this study was located in the United States Forest Service's National Talladega Forest near Centreville, Alabama (32.90289°, −87.24968°, and 126 m elevation). This site is part of the Southern Aerosol Research and Characterization network (SEARCH), where Atmospheric Research and Analysis, Inc. (ARA) has been collecting data on US Environmental Protection Agency (EPA) criteria gas and aerosol species since the early 1990s (http://www.atmospheric-research.com/studies/SEARCH/).

Due to its location in a heavily forested area, Centreville is primarily a rural site with high biogenic emissions from a mixture of conifer and deciduous trees. Its proximity to Birmingham, AL, located 71 km northeast of Centreville, causes the site to be influenced by elevated anthropogenic NO_x emissions. In addition, numerous coal-fired power plants in the region, including four within an 80 km radius, generate high point source SO_2 and NO_x emissions that raise concentrations of these pollutants when the wind direction transports those plumes to the site (see Fig. S1 in the Supplement).

2.2 Aerosol and gas composition

2.2.1 Bulk composition analysis via Monitor for Aerosols and Gases

Inorganic gas and aerosol composition at the SOAS site was characterized using a Monitor for AeRosols and GAses (MARGA) (Metrohm Applikon BV, Netherlands). The MARGA is a semi-continuous ion chromatography instrument designed to measure ambient concentrations of inorganic particulate matter (PM) and gases. Species detected by MARGA include gas phase HCl, HNO_3, HONO, NH_3, and SO_2, and particulate Cl^-, NO_3^-, SO_4^{2-}, NH_4^+, Na^+, K^+, Mg^{2+}, and Ca^{2+}. The MARGA inlet employs a wet rotating denuder (WRD) and a steam jet aerosol collector (SJAC), for collection of gases and particles, respectively, in con-

Table 1. Statistical summary of major gas and particle phase species measured by the MARGA. Concentrations ($\mu g\,m^{-3}$) of each species were collected from 1 June to 13 July 2013 ($n = 949$) and were averaged over 1 hour of sample collection.

Species	MDL[a]	Mean (±1σ standard deviation)	Minimum	Maximum
HNO_3	0.05	0.34 ± 0.14	[b]	1.14
NH_3	0.05	0.51 ± 0.24	0.15	2.09
SO_2	0.04	0.68 ± 1.47	[b]	16.4
Cl^-	0.02	0.02 ± 0.05	[b]	0.42
NO_3^-	0.04	0.37 ± 0.20	[b]	1.07
SO_4^{2-}	0.03	2.20 ± 1.19	0.50	8.87
NH_4^+	0.03	0.67 ± 0.38	0.11	2.21
Na^+	0.02	0.08 ± 0.09	[b]	0.50
K^+	0.01	0.05 ± 0.06	[b]	0.31
Mg^{2+}	0.01	0.01 ± 0.02	[b]	0.09
Ca^{2+}	0.01	0.05 ± 0.06	[b]	0.31

[a] minimum detection limit (MDL) as reported by Makkonen et al. (2012).
[b] Below minimum detection limit (MDL).

junction with cation and anion chromatography to report gas and aerosol concentrations at an hourly time resolution. The technique, including experimental detection limits, has been described in detail in Makkonen et al. (2012) and Rumsey et al. (2014). Table 1 presents a statistical summary of the MARGA measurements taken during the SOAS campaign.

At the SOAS ground site, ambient air was drawn through a PM_{10} (particles less than 10 μm in diameter) cyclone (Teflon-coated, URG, Chapel Hill, NC), approximately 4 m above ground level, at a flow rate of 16.7 standard L min^{-1}. The sample air flowed through a 196 cm stretch of 2.70 cm inner diameter Teflon-coated aluminum at ambient temperature before reaching a $PM_{2.5}$ (particles less than 2.5 μm in diameter) cyclone (Teflon-coated, URG, Chapel Hill NC). A further 147 cm length of 0.95 cm inner diameter polyethylene tubing at shelter temperature brought the ambient air to the sample box. In total, the inlet had a sample volume of 1224 cm^3 and a residence time of 4.4 s. Losses from the instrument tubing are estimated at less than 5 % for HNO_3 (using Eq. 2 from Trebs et al. (2004) and assuming that HNO_3 has an uptake coefficient of 0.05 on liquid H_2O surfaces from Sander et al., 2011) and less than 1.5 % for particles between 0.25 and 2.5 μm (von der Weiden et al., 2009).

Once at the sample box, the sample air passed through the WRD, in which an absorption solution (10 ppm hydrogen peroxide, used as a biocide, in 18.2 MΩ deionized water) forms a thin aqueous film between two concentric rotating glass cylinders (Keuken et al., 1988). Water-soluble gases diffuse into the absorbance solution while particles continue to the SJAC. The SJAC maintains a supersaturated environment with the absorbance solution, in which particles activate and grow to micro-droplets and are then subsequently collected by inertial separation (Slanina et al., 2001).

Aqueous streams leading from the WRD and the SJAC accumulate for 60 min in separate 25 mL syringes. Once filled, the syringes inject the sample simultaneously with a 2.5 mL Li^+ and Br^- (320 and 3680 $\mu g\,L^{-1}$, respectively) internal standard into a 250 μL anion and a 500 μL cation injection loop before reaching the ion columns. The Li^+ and Br^- standards act as a continuous calibration of all reported data, and allow for automatic adjustments to be made for the age and history of the chromatographic column, such as by using a temperature-controlled oven around each column to ensure chromatographic peaks remain separated. A Metrosep C4 (100×4.0 mm) cation column, in conjunction with 3.2 $mmol\,L^{-1}$ HNO_3 eluent and conductivity detector (Metrohm USA, Riverview, FL), separates and quantifies cationic species in the gas and the particle samples. Similarly, a Metrosep A Supp 10 (75×4.0 mm) column with Na_2CO_3–$NaHCO_3$ (7 and 8 $mmol\,L^{-1}$, respectively) eluent and conductivity detector is used for detection of anions. During analysis, a second set of syringes acts in tandem configuration to collect sample for the next hour. H_3PO_4 is used to regenerate the chemical suppressor after analysis of each sample.

2.2.2   Single-particle analysis via CCSEM and EDX

Samples for single-particle analysis were collected using a multiple orifice uniform deposition impactor (MOUDI; MSP Corp. Model 110) sampling at 30 $L\,min^{-1}$. The MOUDI sampled particles from 0.1 to 10 μm using a PM_{10} cyclone at an elevation of 1 m a.g.l. Samples were typically collected every 11 h, except for brief intensive periods (such as during 10–12 June) when samples were collected every 3 h to give better time resolution. Particles were impacted on 200 mesh Carbon Type B with Formvar grids (Ted Pella Inc.) for analysis by computer-controlled scanning electron microscope (CCSEM) measurements with an FEI Quanta environmental dual focused ion beam scanning electron microscopy (FIB/SEM) equipped with a field emission gun operating at 20 kV and a high angle annular dark field (HAADF) detector (Laskin et al., 2002, 2006, 2012). The instrument was equipped with an energy dispersive X-ray (EDX) spectrometer (EDAX, Inc.), which allows for X-ray detection of elements with atomic numbers higher than Be. For the SOAS field campaign, 43 784 particles were analyzed. The CCSEM automated analysis captured single-particle physical properties including average diameter, projected area, and perimeter. EDX spectra from individual particles were also collected to determine the relative abundance of 22 elements: C, N, O, Na, Mg, Al, Si, P, S, Cl, Ag, K, Ca, Ti, V, Cr, Mn, Fe, Co, Ni, Zn, and Hg. Interferences from the TEM grid (C and O) and the HAADF detector (Si) were present. N could not be quantified due to interference from C, O, and the Bremsstrahlung background.

Single-particle analysis from the CCSEM-EDX was performed in MATLAB R2013b (Mathworks, Inc.) using *k*-means clustering of the elemental composition following the method previously described in Ault et al. (2012). Clusters were grouped into source-based classes by elemental composition, including crustal dust and sea spray aerosol (SSA). Crustal dust particles were characterized by high fractions and intensities of Al and Si, along with other crustal elements including Mg, Ca, K, Ti, and Fe (Sobanska et al., 2003; Krueger et al., 2004; Laskin et al., 2005b; Coz et al., 2009). Sea spray aerosol particles were characterized by the presence of Na and Mg in an approximately 10 : 1 ratio (Culkin and Cox, 1976; Pilson, 1998), which is the ratio of the two cations in seawater, along with K and Ca at appropriate ratios when detected during the 10–15 s EDX spectrum collection throughout CCSEM analysis. The fingerprint to identify SSA is based on laboratory and field studies of seawater generated SSA using SEM (Hopkins et al., 2008; Laskin et al., 2012; Ault et al., 2013b), including after reaction with HNO_3 (Liu et al., 2007; Ault et al., 2013a). Crustal dust was identified through fingerprints from previous studies, including Al, Si, and cation peaks (Na, Mg, K, and Ca) (Edgerton et al., 2009; Ault et al., 2012). Biomass burning was identified by C, O, K, and S (Posfai et al., 2003; Li et al., 2003; Edgerton et al., 2009; Moffet et al., 2010, 2013). SOA (secondary organic aerosol) was composed of different combinations of C, N, O, and S, which will be discussed further in a forthcoming publication with Raman microspectroscopy analysis (Moffet et al., 2010, 2013). Fly ash was determined through a combination of composition and shape analysis (Edgerton et al., 2009; Ault et al., 2012). Industrial particles contained transition or heavier metals (Utsunomiya et al., 2004). Biological particles contained a mix of K, Ca, P, C (very high levels), and O (Edgerton et al., 2009; Huffman et al., 2012; Moffet et al., 2013). Soot was identified through composition (C and O), as well as morphology (Edgerton et al., 2009).

2.2.3   Elemental analysis via XRF

Elemental analysis of $PM_{2.5}$ collected on Teflon filters was performed via energy dispersive X-Ray fluorescence (XRF) using a PANalytical (Westborough, MA) Epsilon-5 ED-XRF spectrometer. The inlet for sample filters was situated 5 m above ground level with a flow rate of 1.25 $L\,min^{-1}$. Sample air is pulled through two annular denuders in series (sodium bicarbonate and citric acid) then collected on a 47 mm diameter, 2 μm nominal pore size-ringed Teflon filter. The Epsilon-5 was calibrated with MicroMatter (Vancouver, BC) XRF single element calibration standards, which are prepared by vacuum deposition on a polycarbonate substrate, resulting in a uniform deposit of the element with a nominal loading of 50 ± 2.5 $\mu g\,cm^{-2}$. The results from the MicroMatter standards are then compared with the field samples containing 0.1–5 $\mu g\,cm^{-2}$ pollutant (Edgerton et al., 2005). The detection limits (minimum detection limit – MDL) were determined from field blank loadings assuming nominal sample volume of 24 m^3. Measurement precision was estimated
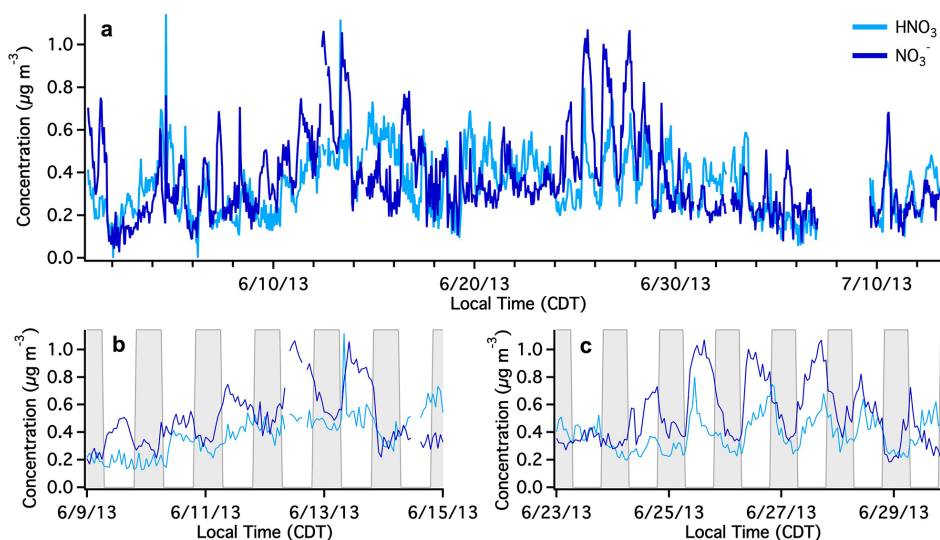
Figure 1. Time series of hourly averaged HNO_3 and NO_3^- concentrations measured by MARGA during the summer SOAS campaign, including the **(a)** full time series and two subsets, with shading indicating nighttime, that encompass the periods of elevated NO_3^- during **(b)** 9 to 15 June and **(c)** 23 to 30 June 2013.

from routine replicate analysis and from the average relative standard deviation (RSD) of triplicate analyses from a subset of samples collected during the study. Accuracy was assessed using NIST-2783 (Air Particulate on Filter Media) and internally generated standards using a research-grade deposition chamber and verification protocol employing inductively coupled plasma mass spectrometery (ICP-MS; Kul/ARA 0802A18 QCCHK) (Kulkarni, 2010).

2.2.4 Particle size via SMPS and APS

Particle size distributions were measured over the diameter range 0.01–20 µm with a scanning mobility particle sizer (SMPS; 0.01–0.7 µm diameter; TSI Inc., Shoreview, MN, model 3080 consisting of a TSI model 3081 DMA and TSI model 3772 CPC), and an aerodynamic particle sizer (APS; 0.5–20 µm diameter; TSI model 3321). The instruments were operated outdoors in a ventilated tent to ensure that the temperature (and therefore relative humidity and particle size) was near ambient conditions. Vertically oriented, stainless steel tubes (length 1.4 m, OD 0.25 in, ID 0.18 in) connected the SMPS inlet (flow rate $1 \, \text{L} \, \text{min}^{-1}$) and inner APS inlet (flow rate $1 \, \text{L} \, \text{min}^{-1}$) to a common, stainless steel inlet with a purpose-built rain hat above the tent. A particle density of $1 \, \text{g} \, \text{cm}^{-3}$ and shape factor of 1 (corresponding to wet aerosols) were assumed for merging the SMPS and APS size distributions (Khlystov et al., 2004), and for calculating the integrated mass concentrations of PM_1 and $PM_{2.5}$.

2.2.5 Modeling via ISORROPIA and E-AIM

ISORROPIA II, a thermodynamic equilibrium model for inorganic gases and aerosols in the atmosphere (available at http://isorropia.eas.gatech.edu) was employed to assess the equilibrium state of the aerosol found at Centreville, as well as to check the model's ability to accurately capture gas–aerosol chemistry in the atmosphere at Centreville. Concentrations of inorganic species measured with an hourly time resolution by MARGA were input into the model as total (gas + aerosol) concentrations: SO_4^{2-}, $HNO_3 + NO_3^-$, $NH_3 + NH_4^+$, Na^+, $HCl + Cl^-$, Ca^{2+}, K^+, and Mg^{2+}, along with temperature and relative humidity (RH) measurements. Temperature and RH measurements were collected at 1 min resolution from the ARA SEARCH monitoring site collocated with the SOAS ground site at Centreville (approximately 10 m from the MARGA site; Fig. S2). The meteorological sensor was mounted 9 m above ground and employed a MET4 sensor probe (Paroscientific Inc, Redmond, WA) with 0.1 4 °C and 0.8 % accuracy for temperature and RH, respectively (Hansen et al., 2003). The meteorological data were averaged to hourly increments to match the time resolution of MARGA measurements input into the model. ISORROPIA II was run in the "forward" mode in the thermodynamically stable state, in which the model repartitions the gas and aerosol-phase species assuming thermodynamic equilibrium conditions and salts precipitate once the aqueous phase becomes saturated, in order to determine if each species would be present in the gas, aerosol, or solid phases (Fountoukis and Nenes, 2007). E-AIM (Extended Aerosol Inorganics Model; available at http://www.aim.env.uea.ac.uk/aim/aim.php) model IV was similarly employed (inputs

of total gas + aerosol concentrations of SO_4^{2-}, $HNO_3+NO_3^-$, $NH_3+NH_4^+$, Na^+, and $HCl+Cl^-$, temperature, and RH with the model configured to allow salts to precipitate once the aqueous solution becomes saturated), but does not include the mineral species Ca^{2+}, K^+, and Mg^{2+} (Wexler and Clegg, 2007). E-AIM simulations require ion balance of all analytes; thus, any cation deficiency was balanced using inputs of H^+. The sensitivity of the E-AIM model to variability in major analytes and to the ion balancing approach has been shown to be relatively minor (Young et al., 2013).

3 Results and discussion

3.1 Overview

During the SOAS campaign, HNO_3 and NO_3^- concentrations were relatively low compared to other inorganic ions such as sulfate and ammonium. Figure 1 presents the time series of HNO_3 and NO_3^- measurements between 1 June and 15 July 2013, along with subsets (Fig. 1b and c) indicating concentrations during periods of high NO_3^- concentrations. Gas phase HNO_3 concentrations averaged $0.34\,\mu g\,m^{-3}$ (0.14 ppb), with a maximum of $1.14\,\mu g\,m^{-3}$ (0.46 ppb) and a minimum of $0\,\mu g\,m^{-3}$ (0 ppb) (Table 1), and were typically highest during the early to late afternoon. The peak afternoon HNO_3 concentrations likely resulted from the increase in temperature that occurs between nighttime to daytime, which enhances nitrate evaporation to the gas phase as HNO_3. In addition, daytime photochemical production of HNO_3 from NO_x chemistry and the enhanced aerosol acidity from photochemical production and subsequent condensation of other soluble acids (e.g., H_2SO_4 from SO_2 oxidation) likely contributed to the observed day–night variability of HNO_3 as well.

Aerosol NO_3^- exhibited an average concentration of $0.38\,\mu g\,m^{-3}$, ranging from 0.03 to $1.07\,\mu g\,m^{-3}$ (Table 1), and typically peaked in the late morning to early afternoon. The higher daytime aerosol-phase nitrate concentrations indicate most NO_3^- is likely formed from the reaction of NO_2 via the daytime oxidant, OH. N_2O_5, which produces nighttime HNO_3 via hydrolysis, was measured at the field site, but due to slow N_2O_5 hydrolysis rates and high concentrations of organics in the surrounding area, likely contributed little to HNO_3 formation (Ayres et al., 2015). Periods of high NO_3^- concentrations ended when significant rainfall (3.5 mm of rain on 13 June and 1.9 mm on 28 June) removed aerosol from the air.

However, collocated HNO_3 and NO_3^- instruments observed notable variations in measurements of these two species. The routine monitoring of HNO_3 by ARA's SEARCH network instrument indicates higher daytime concentrations of HNO_3 relative to the MARGA. Another measurement of HNO_3 via chemical ionization mass spectrometry atop a 20 m tower near the ground-based measure-
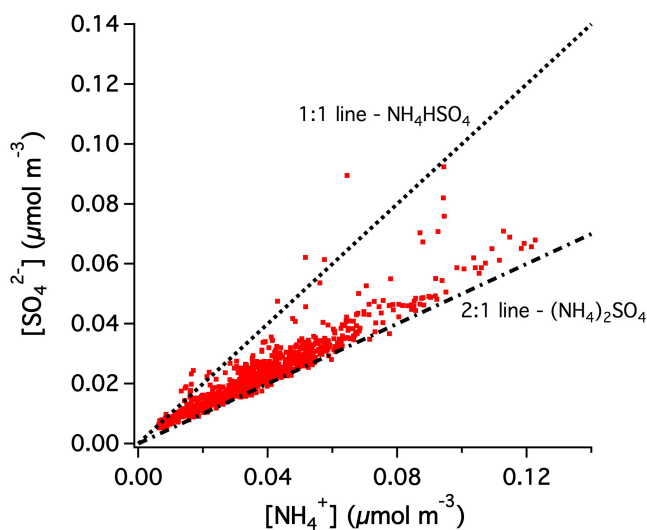

Figure 2. Correlation of SO_4^{2-} and NH_4^+ concentrations measured by MARGA during the 2013 SOAS campaign (1 June to 13 July). The higher concentrations of SO_4^{2-} relative to NH_4^+ show an acidic environment at the SOAS site, with insufficient moles of NH_4^+ present to fully balance existing SO_4^{2-} as $(NH_4)_2SO_4$.

ments gave concentrations more similar to those reported by the MARGA. The observed range of HNO_3 concentrations does not substantially affect the conclusions of this analysis (Sect. 3.5). In addition, comparison of NO_3^- measurements indicates that measurements of this species may be influenced by minor differences in the cut point of sample inlets. The MARGA, which sampled with a $PM_{2.5}$ cyclone, measured substantially higher NO_3^- concentrations than similar measurements made by an aerosol mass spectrometer with a PM_1 size cut. The MARGA also measured higher NO_3^- than the ARA's $PM_{2.5}$ instrument, likely due to incomplete separation efficiency by the MARGA's $PM_{2.5}$ cyclone. The importance of size cut is discussed in Sect. 3.2; see Supplement for a complete description and comparison of these data sets.

The high observed concentrations of sulfate lead to highly acidic aerosol in the atmosphere of the southeastern United States during the SOAS campaign. The correlation of SO_4^{2-} with NH_4^+ concentrations shows that the observed ammonium concentrations are insufficient to fully balance the existing sulfate (Fig. 2). Centreville is located in a region with numerous coal-fired power plants, leading to high concentrations of SO_4^{2-}, with an observed summertime range of 0.50–$8.87\,\mu g\,m^{-3}$. Of the inorganic ions, SO_4^{2-} dominated the aerosol-phase ionic composition and led to the highly acidic nature of the aerosol. The H^+ concentration was calculated by subtracting total charge equivalents of anions from that of cations in $\mu mol\,m^{-3}$:

$$H^+ = [Cl^- + NO_3^- + 2 \times SO_4^{2-}]$$
$$- [Na^+ + NH_4^+ + K^+ + 2 \times Mg^{2+} + 2 \times Ca^{2+}]. \quad (1)$$

The average inferred H$^+$ concentration at the site was 8 ± 6 nmol m^{-3}, with a range of 0 to 109 nmol m^{-3}, indicating a cation deficiency and therefore acidic aerosol. However, the variable effects of liquid water, the buffering action of HSO$_4^-$ / SO$_4^{2-}$, and the effect of species activity coefficients prevents an accurate measure of pH from the H$^+$ inferred by ion balance (Hennigan et al., 2015). In addition, because the inferred H$^+$ concentration is calculated from analytes measured as a mixture of potentially chemically distinct size fractions and does not include H$^+$ contributed by organic species or other acids, it is not necessarily representative of all corresponding size fractions in ambient air and is likely a lower limit estimate. The high acidity found in this study is in agreement with Guo et al. (2015), who give a detailed study of acidity at the SOAS site and report a mean pH of 0.94 ± 0.59 and a diurnal mean H$^+$ concentration between 0.5 and 2.5 nmol m^{-3} at the SOAS ground site. The acidities measured by MARGA and modeled by Guo et al. (2015) are consistent with that of aerosol characterized as acidic in several other urban and non-urban studies (Koutrakis et al., 1988; Spengler et al., 1989; Brauer et al., 1991; Lee et al., 2008).

Modeling of the inorganic ionic species by ISORROPIA II, which utilizes all inorganic ionic species measured, including mineral species, produced an average predicted H$^+$ concentration of 0.32 nmol m^{-3} and a range of < 0.00 to 12.00 nmol m^{-3} of H$^+$, up to an order of magnitude lower than values inferred from MARGA measurements. The discrepancy between measured and modeled acidity likely arises from the difference between total acidity (obtained by ion balance assuming full dissociation of acids as done with measurements above) and free acidity (obtained by calculating the extent of dissociation as provided by ISORROPIA II), as well as from differences in treatment of aerosol liquid water content and the H$^+$ activity coefficient, which ion balance does not take into account (Hennigan et al., 2015). Hydrogen ion concentrations calculated by ion balance are often higher than those estimated by models due to these differences (Saxena et al., 1993; Guo et al., 2015).

The observed acidity likely served to suppress aerosol NO$_3^-$ formation, as high acidity is indicative of an atmosphere deficient in the cations necessary to allow nitrate to partition into the aerosol phase. The limited NH$_3$ at the site will mostly associate with the acidic submicron sulfate, producing fine mode (NH$_4$)$_2$SO$_4$ or NH$_4$HSO$_4$ aerosol (Fig. 2). The formation of fine-mode aerosol NO$_3^-$ is therefore limited, as only the NH$_4^+$ not already associated with sulfate will be free for the potential formation of NH$_4$NO$_3$. Most nitrate will therefore likely partition, given temperature and equilibrium constraints, into the gas phase as HNO$_3$. The observed

high ratio of gas phase HNO$_3$ to aerosol NO$_3^-$ is consistent with these high acidity observations. However, as explored in the next section, a substantial amount of NO$_3^-$ aerosol was able to form on supermicron aerosol rather than fine mode due to the presence of other aerosol cation species.

3.2 Influence of crustal dust and sea spray on nitrate aerosol

Two periods occurred from 9 to 13 June (designated "coarse particle event 1") and 23 to 28 June 2013 (designated "coarse particle event 2"), in which unusually high aerosol NO$_3^-$ was observed. These two events correspond with an increase in mineral species such as Na$^+$, Ca^{2+}, Mg^{2+}, and K$^+$, suggesting that during these periods, the mineral cations decreased aerosol acidity enough to drive HNO$_3$ into the aerosol phase as supermicron NO$_3^-$ (Fig. 3). NO$_3^-$ concentrations track with variations in the concentrations of these mineral cations, enough of which are present to fully balance NO$_3^-$ on a charge equivalent basis (Fig. 3c), although not enough to balance both NO$_3^-$ and non-ammonia associated SO$_4^{2-}$ anions.

The close correlation between the observed trends of aerosol NO$_3^-$ and Na$^+$ and Ca^{2+} indicate that NO$_3^-$ predominately forms during times of high mineral species, likely by reactions on the surface of sea spray and crustal dust. During the beginning of coarse particle event 1, particularly around 9 and 10 June, relatively high concentrations of Cl$^-$ were present with Na$^+$. Over a period of 5 days, Cl$^-$ gradually diminished in the aerosol while NO$_3^-$ and HCl concentrations increased (Fig. 3b). The reaction of HNO$_3$ on sea spray reaches equilibrium on the order of several hours to a day for particles between 1.0 and 2.5 μm in diameter (Evans et al., 2004). The decreased concentrations of Cl$^-$ over the course of several days during the first event thus suggests the reaction of HNO$_3$ on sea spray surfaces and subsequent volatilization of aerosol Cl$^-$ to HCl as the air mass aged.

Observations of aerosol size distribution during the first event suggest the role of both sea spray and crustal dust in aerosol NO$_3^-$ formation, as the high NO$_3^-$ events corresponded to a shift in particle size towards aerosols with larger diameters (Fig. 3a). Between 9 and 13 June, aerosols with diameters in the 1–2.5 μm range (PM$_1$–PM$_{2.5}$) were more prevalent than those with diameters less than 1 μm (PM$_1$) (Fig. 3a). The increase towards higher diameter particles correspond to a similar increase in the concentrations of both crustal dust and sea spray species, such as Na$^+$ and Ca^{2+}, and of NO$_3^-$. Although PM$_1$–PM$_{2.5}$ size data were not available during the second event, the increase in mineral species suggests that a similar shift towards increasing mineral dust or sea salt aerosol in this size regime occurred during coarse particle event 2 as well. The increase in mineral species and shift in aerosol diameter suggest that aerosol NO$_3^-$ formation occurs as supermicron NaNO$_3$ and Ca(NO$_3$)$_2$.
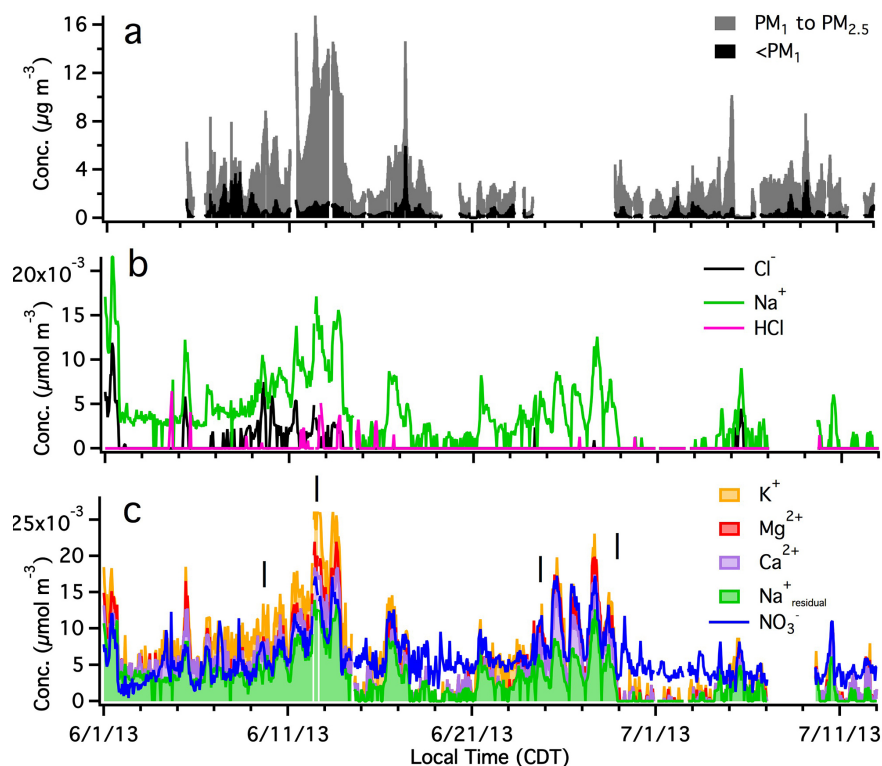
Figure 3. Observations of high aerosol NO_3^- during the SOAS campaign correlated with **(a)** high PM_1–$PM_{2.5}$ hydrated aerosol mass fraction during coarse particle event 1; **(b)** high Na^+ concentrations during both events, and Cl^- and HCl concentrations during the first event; and **(c**, stacked) high concentrations of mineral cations during both events, indicating that NO_3^- likely formed on the surfaces of sea spray and crustal dust during these two events. $Na_{residual}^+$ indicates aerosol Na^+ not associated with Cl^-, calculated by subtracting an equivalent of Cl^- from Na^+. The dates indicated by vertical lines in **(c)** were chosen for wind pattern analysis (Sect. 3.3).

3.3 Mineral species origin

MARGA and XRF measurements of mineral species suggest that the mixture of both reacted crustal dust and sea spray is important for aerosol NO_3^- formation, yet the two coarse particle events exhibited differences in their mineral composition. The first event appears to be more strongly influenced by sea spray transport, as Cl^- existed in significantly higher concentrations during this event than at any other time during the campaign. The first coarse particle event exhibited a higher percentage of Na^+ (12 %) than occurred during the second event (7.5 %), and the second event had no accompanying Cl^- as indicated by Fig. 3. However, the lack of observed Cl^- during the 23–28 June event may be due to a longer air mass transport that provided sufficient time for Cl^- depletion, which occurs on the order of many hours to a day, to happen before the air mass reached the sampling site. The low Mg^{2+} to Na^+ molar ratio (0.08) during the first event relative to seawater (0.114) also suggests a non-sea-salt origin for at least some of the Na^+ observed at this time (Jordan et al., 2015). The second event had a higher percent composition of Ca^{2+} (3.3 %) than was present during the first event (2.4 %) (Table 2), as well as a larger Ca^{2+}

to Na^+ ratio (0.302 for the first event and 0.509 for the second; for comparison, the Ca^{2+}/Na^+ of seawater is 0.022; Jordan et al., 2015), suggesting that the second event was likely more influenced by crustal dust. Although some crustal dust does contain Na^+ and Cl^- concentrations in ratios similar to those in sea spray (Young et al., 2013; Jordan et al., 2015), further analysis by CCSEM and EDX shows that, averaged over all particle diameters, during the first coarse particle event (12 samples) 27 % of aerosols were crustal dust and 20 % were sea spray, while during the second coarse particle event (3 samples) 53 % of particles were crustal dust and 23 % were sea spray. These measurements support the conclusion that the first event was more strongly influenced by sea spray while the second event was more strongly influenced by crustal dust.

Back trajectory analysis of the air mass origin during the two coarse particle events was conducted to elucidate the origin of the mineral species. The trajectories were computed using version 9.0 of the FLEXible PARTicle dispersion model (FLEXPART; Stohl et al., 1998; available at http://flexpart.eu/), driven by analysis of the Global Forecasting System (GFS) of the National Centers for Environmental Protection (NCEP). The calculations were conducted by ran-

Table 2. Percent composition of mineral species and element : Si ratios during the two coarse particle events observed during the summer 2013 SOAS field campaign.

Element	MDL* ($\mu g\,m^{-3}$)	Coarse particle event 1		Coarse particle event 2	
		Composition (%)	Si ratio	Composition (%)	Si ratio
Al	0.006	27 %	0.64	26 %	0.59
Si	0.006	42 %	1	45 %	1
K	0.007	5 %	0.12	6 %	0.11
Ca	0.004	2 %	0.06	3 %	0.07
Ti	0.0003	1 %	0.03	1 %	0.02
Mn	0.0012	< 1 %	< 0.01	< 1 %	< 0.01
Fe	0.0014	9 %	0.22	9 %	0.21
Na^+	0.02	12 %	0.31	8 %	0.18
Mg^{2+}	0.01	1 %	0.02	2 %	0.04

Al, Si, K, Ca, Ti, Mn, and Fe data from ARA XRF measurements; Na and Mg from MARGA data measurements; all have 2.5 μm size cut. * minimum detection limit (MDL)

domly releasing 10 000 inert air parcels within a 3 h period from the location of the Centreville, AL, site, and followed for 3 days. This resulted in time-resolved 3-D information on the location of the air mass prior to arrival at Centreville, AL, including uncertainty due to stochastic processes like convection or turbulence acting on the air mass. From this information, deterministic trajectories were calculated to better guide the reader. Selected results of the back trajectory analysis are presented in Fig. 4.

The wind back trajectory analysis shows similar wind patterns occurring during the two coarse particle events. At the beginning of both events, winds originated from the Gulf of Mexico and traveled north to reach the measurement site. As the events continued, wind patterns shifted and the air mass arrived from Texas traveling westwards along the continental United States until, near the end of each event, the air mass originated from a high elevation near the western coast of the United States. Although the overall pattern in wind trajectories is similar between the two coarse particle events, slight differences in the wind patterns at the beginning of each event may have contributed to the observed differences in composition of the aerosol. The air mass at the beginning of coarse particle event 1 traveled at low elevation (500–1000 m a.s.l.) across the Gulf of Mexico and continued at this elevation until reaching the site, thus likely collecting and transporting sea spray aerosol to Centreville (Fig. 4a). In contrast, the air mass from event 2 originated from the northern shore of the Gulf and traveled at a lower elevation over land (less than 500 m a.s.l.) and was over land for a greater period of time (Fig. 4c). Estimates of marine aerosol lifetimes suggest that the lifetime of these aerosol against deposition is on the order of 0.5 to 2 days (Jordan et al., 2015), indicating that any marine aerosol collected during the second event had likely undergone deposition from the air mass before reaching the SOAS site. These observations accord with the greater influence of marine aerosols on the first coarse particle event compared to the second (Fig. 3), and suggest a

relatively local (within the United States) origin of the crustal dust aerosol.

3.4 Single-particle composition evidence for coarse-mode HNO₃ uptake

Individual particle analysis using CCSEM for the two coarse particle events was compared with the remainder of the campaign. Particle classes, determined from cluster analysis of EDX spectra, showed that the two coarse particle events contained a significantly higher percentage of crustal dust and sea spray aerosol, particularly in the supermicron size range, than was otherwise present during the course of the campaign (Fig. 5). During the two coarse particle events, between 15 and 20 % of submicron particles and between 30 and 50 % of supermicron particles consisted of crustal dust. By comparison, outside of these two events less than 5 % of fine-mode particles analyzed and between 10 and 25 % of supermicron particles consisted of crustal dust. The percentage of crustal dust and sea spray during the two events (27 and 20 % for event 1, and 53 and 23 % for event 2) are higher than those throughout the entire field study (5 June to 11 July 2013), in which 17 % of particles were crustal dust and 16 % were sea spray. The sizes of dust and marine particles during event versus non-event periods are comparable and particles were both externally and internally mixed. However, because fewer samples were available for analysis for event 2, there is greater error associated with the relative aerosol composition for this period. As a result of the larger fraction of crustal dust and sea spray during these events, the relative fraction of secondary organic aerosol decreases from the majority (more than 50 %) of particles in the 1–2 μm range during non-coarse events to a significantly smaller fraction (approximately 25 %) of particles in the same diameter range during the coarse events.

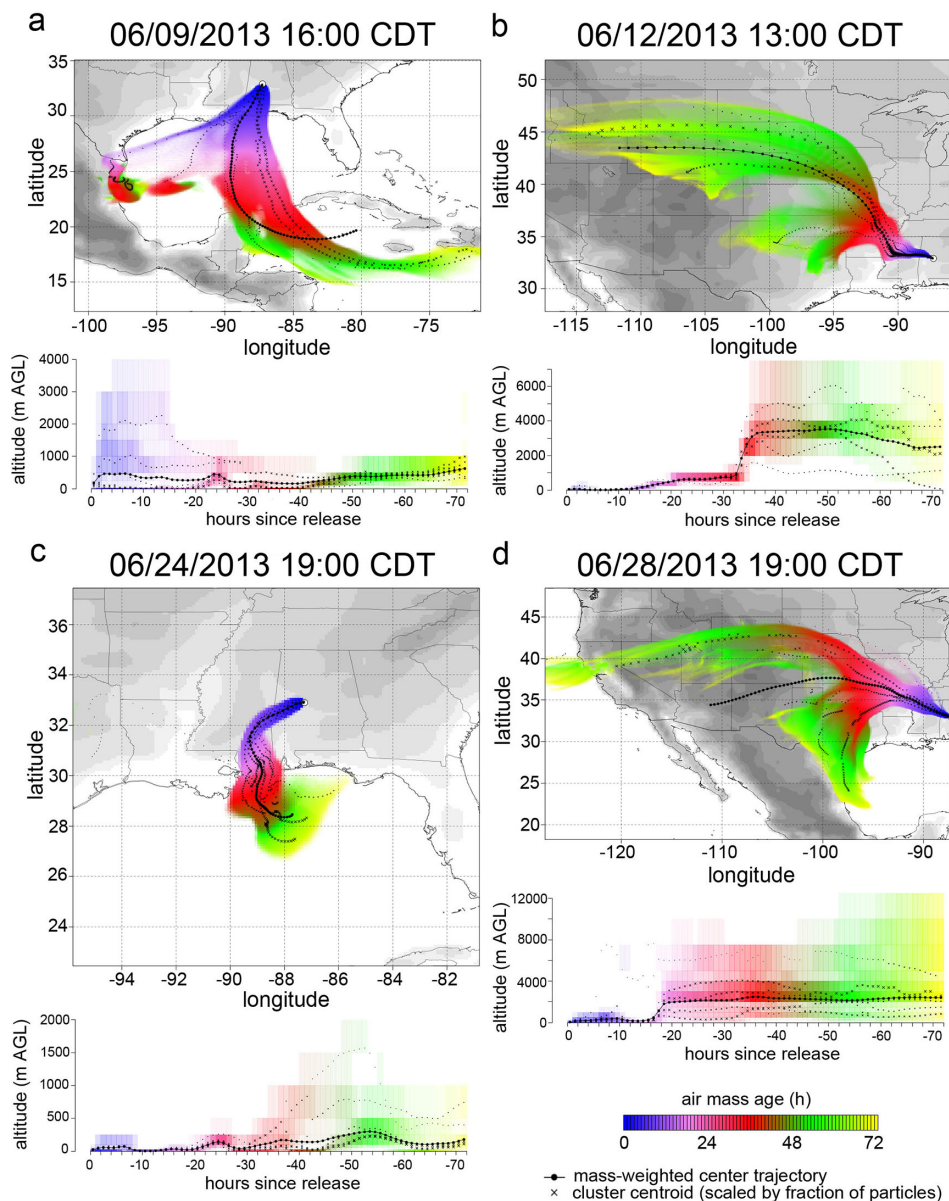SEM with EDX was also used to investigate the contribution of total nitrogen (including both inorganic and organic

Figure 4. Shown are 3-day back trajectories at the Centreville site (circled), displaying horizontally integrated (top) and vertically integrated (bottom) trajectories with mass-weighted and cluster centroid trajectories as defined by Stohl et al. (2002), for **(a)** event 1 on 9 June, **(b)** event 1 on 12 June, **(c)** event 2 on 24 June, and **(d)** event 2 on 28 June. Times shown correlate with peaks indicated by vertical bars in Fig. 3c.

present, assuming minimal losses under the vacuum of the SEM as nitrogen was most frequently found in the fairly non-volatile form of NaNO$_3$; Laskin et al., 2002, 2005a) to particles collected during the campaign. The average weight percent of nitrogen per particle during the coarse particle events and non-coarse particle events varied as a function of particle diameter. Overall, a higher atomic weight percent of nitrogen was present in particles with diameters larger than 1 µm. In addition, the average number fraction of sea spray aerosol + crustal dust was similarly the highest for supermicron particles, increasing substantially for particles 1 µm or larger in

diameter. The mixing of nitrate in sea spray aerosol will be described in detail in a forthcoming publication (Bondy et al., 2015). These data thus corroborate previous analysis on the impact of high acidity at the site by showing that very little nitrogen occurs in the fine mode in the aerosol, and indicate the importance of crustal dust and sea spray aerosol in larger diameter particles.

3.5 Rate of nitrate production

In order to assess the contribution of mineral cations to aerosol NO$_3^-$ formation, the rate of the heterogeneous up-
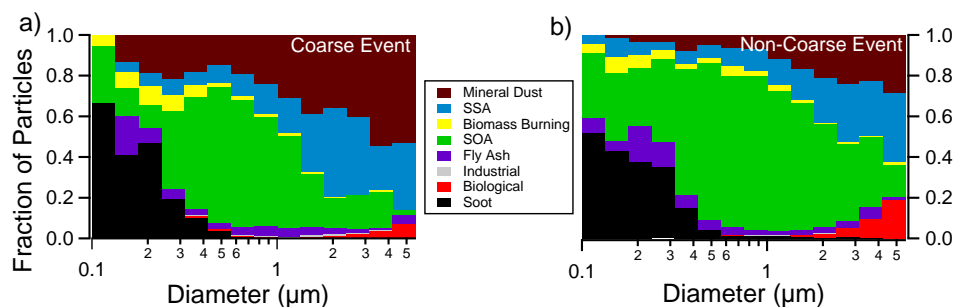
Figure 5. Compositional analysis using SEM with EDX of particles collected during the SOAS campaign as a function of particle diameter during **(a)** the two coarse particle events and **(b)** throughout the remainder of the field campaign. SSA indicates sea spray aerosol and SOA indicates secondary organic aerosol.

take of HNO_3 onto aerosol to form NO_3^- was determined using the Fuchs–Sutugin approach (Fuchs and Sutugin, 1971). This approach estimates the transition regime rate of uptake of HNO_3 onto measured aerosol surface area per unit volume:

$$\text{Rate} = \sum_{R_p} \frac{S_a}{R_p} D_g \left(\frac{0.75\alpha(1 + Kn)}{Kn^2 + Kn + 0.283\alpha Kn + 0.75\alpha} \right)[HNO_3], \quad (2)$$

where S_a is the surface area per volume of aerosol in each size bin between 0.7 and 2.5 μm in diameter, R_p is the aerosol particle radius of the size bin, D_g is the diffusivity of HNO_3 in air (0.118 cm^2 s^{-1}, Durham and Stockburger, 1967), α is the accommodation coefficient, assumed to be the same as the kinetic regime measured uptake coefficient (γ, 0.1 for HNO_3, Usher et al., 2003), and Kn is the Knudsen number ($Kn = \frac{3D_g}{c_{HNO_3}R_p}$, $c_{HNO_3} = 341$ m s^{-1} at 298 K). Aerosol size distribution data were available only for the first of the two coarse particle events.

The rate of HNO_3 uptake necessitates the transition-regime approach because the aerosol size range assumed to be important for crustal dust or sea salt uptake, 1–2.5 μm diameter, includes particles large enough to render the transition regime rate more appropriate than the commonly used kinetic uptake expression. A comparison of the rate predicted by Eq. (2) to the kinetic rate uptake expression (rate $= \frac{1}{4}\gamma_{HNO_3}S_a c_{HNO_3}[HNO_3]$) indicates that during peak supermicron-mode loading on 13 June 2013, the transition-regime calculation is approximately 65 % of the rate derived from the kinetic expression.

The calculated rate of HNO_3 uptake onto aerosol surface area supports the conclusion that NO_3^- is produced primarily by this heterogeneous process. Figure 6 shows the calculated rate of production by heterogeneous uptake, along with factors that contribute to the rate of uptake such as S_a and $[SO_4^{2-}]$ (as a proxy for aerosol acidity). The average predicted rate of uptake during the campaign was approximately 0.07 (μg m^{-3}) h^{-1}, but increased to higher than 0.50 (μg m^{-3}) h^{-1} during the first coarse particle event. This increase in the rate of production tracks most closely with a similar increase in the surface area of aerosol between 1
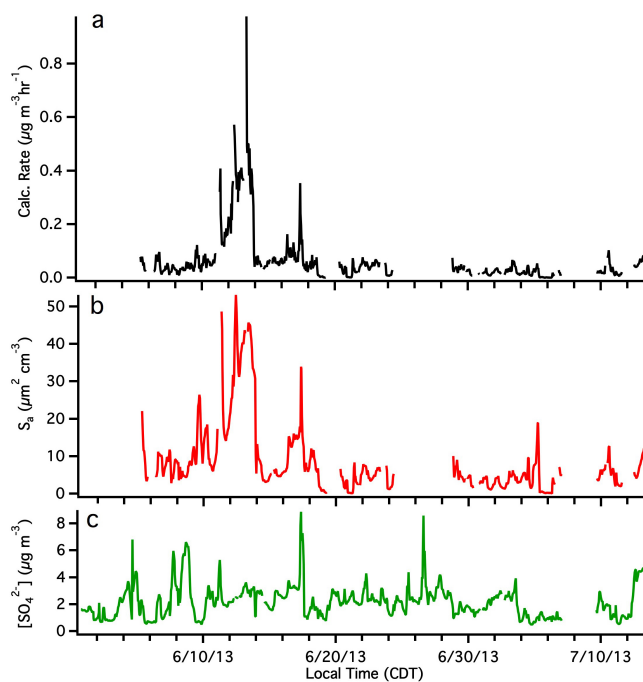

Figure 6. (a) The rate of nitrate production from mineral cations during the 2013 SOAS campaign was calculated from HNO_3 concentrations and **(b)** the estimated aerosol surface area of particles between 0.7–2.5 μm diameters. This rate is compared with factors that contribute to NO_3^- production, such as **(b)** the estimated aerosol surface area and **(c)** SO_4^{2-} concentrations, used as a proxy for aerosol acidity. Higher NO_3^- concentrations (Fig. 1) correlate most strongly with higher $PM_{2.5}$ surface area.

and 2.5 μm in diameter (Fig. 6b) rather than with concentrations of HNO_3 (Fig. 1). As a consequence, using alternate collocated HNO_3 measurements does not affect the predicted aerosol NO_3^- production rates substantially (Fig. S9). The rate of NO_3^- production from this heterogeneous process also appears to correlate well with increases in observed NO_3^- concentrations (Fig. 1), particularly when compared with other factors that may contribute to aerosol NO_3^- for-
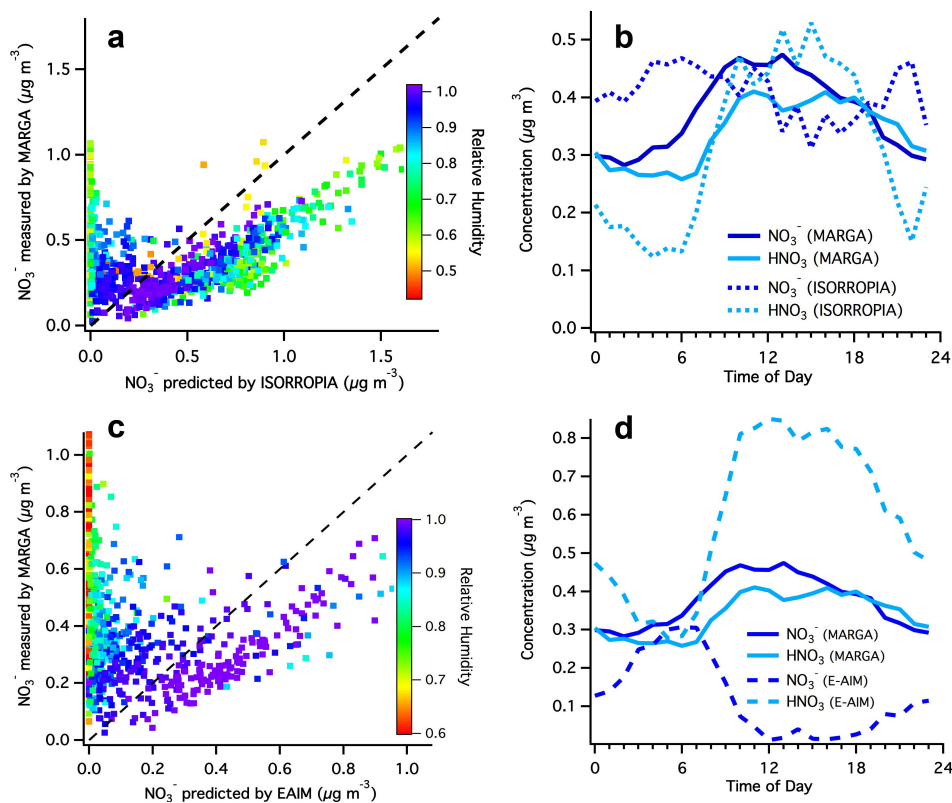
Figure 7. Results of inorganic modeling compared with measurements made by MARGA during the 2013 SOAS campaign. **(a)** Correlation of hourly aerosol NO_3^- concentrations predicted by ISORROPIA II and measured by MARGA; **(b)** Diurnal pattern, averaged over the duration of the campaign, of gaseous HNO_3 and aerosol NO_3^- for ISORROPIA II and MARGA; **(c)** Correlation of hourly aerosol NO_3^- concentrations predicted by E-AIM and measured by MARGA; and **(d)** Diurnal pattern, averaged over the duration of the campaign, of gaseous HNO_3 and aerosol NO_3^- for E-AIM and MARGA.

mation, such as acidity from increased SO_4^{2-} concentrations (Fig. 6c). Thus, the limiting factor contributing to aerosol NO_3^- formation is likely the crustal dust and sea spray surface area. In a companion paper (Ayres et al., 2015), the production rate of inorganic nitrate aerosol is compared to that of organonitrate aerosol from NO_3 radical reactions with biogenic volatile organic compounds (VOC). The rate of inorganic NO_3^- and organonitrate production are comparable in average magnitude, but maximized at different times. Thus, the ultimate aerosol fate of NO_2 depends on the relative prevalence of sea salt or crustal dust versus biogenic emissions.

3.6 Modeling and measurement comparison

The results of the ISORROPIA II and E-AIM models and comparisons with measured values are presented in Fig. 7. The ISORROPIA II model predicted average nitrate chemistry relatively well, as the comparison between NO_3^- measured by MARGA and that predicted by ISORROPIA II shows a linear correlation (Fig. 7a), with a slope of 0.63 ± 0.06. However, ISORROPIA II both under- and over-

predicted NO_3^- with respect to concentrations measured by MARGA, and the correlation produced a low R^2 value of 0.11. The deviations between model and measurement show a moderate relationship with diurnal profile: ISORROPIA II consistently under-predicted particulate NO_3^- concentrations during daylight hours but over-predicted them during the night, with the reverse for gas phase HNO_3 (Fig. 7b).

The importance of explicitly including these mineral species in thermodynamic modeling is highlighted by the results from E-AIM. The model was unable to accurately assess aerosol NO_3^- concentrations, under-predicting concentrations of NO_3^- relative to measurements for the majority of the campaign. Instead, the model partitioned most available nitrate into the gas phase as HNO_3 (Fig. 7c and d). Correlations of modeled and measured aerosol NO_3^- produce an R^2 value of 1×10^{-3}. E-AIM, which includes all mineral species (Ca^{2+}, Mg^{2+}, and K^+) as Na^+ equivalents in its thermodynamic calculations, manifests a strong dependence on RH and a prominent difference in diurnal pattern. Predictions of NO_3^- using thermodynamic models are often very sensitive to inputs of temperature, RH, and available ammonia (Markovic et al., 2011). Only during the nighttime, when RH

values were higher and temperature is lower, does E-AIM partition nitrate into the aerosol phase. The strong diurnal pattern of HNO$_3$ and NO$_3^-$ given by E-AIM, when compared with that of measured temperature (Fig. S3), suggests that the model might rely too heavily upon temperature-driven phase partitioning rather than on other factors that could contribute to this partitioning, such as mineral species. The high temperatures and RH, combined with the acidic atmosphere in the southeastern United States and presence of high mineral aerosol concentrations, mean significant discrepancies may exist between observations and simulations when these mineral species are not explicitly considered in thermodynamic models. These findings are consistent with Trebs et al. (2005) and Metzger et al. (2006), who performed modeling studies of the Amazon and the Mediterranean, respectively, and with Karydis et al. (1988), all of whom similarly found that mineral cations must be explicitly included in inorganic models in order to obtain valid information on gas–aerosol partitioning and ionic balance.

4 Historical trends

Crustal dust and aerosol acidity have been shown to be important factors to consider when seeking to understand the chemistry that occurs in the atmosphere above the southeastern United States. The site chosen for this campaign is part of the SEARCH network, which has been continuously monitoring aerosol and gas composition at Centreville for the past 5 years and thus gives a historical record for assessing the importance of supermicron nitrate in this area. Measurements of PM$_{2.5}$ aerosol species, such as NH$_4^+$, SO$_4^{2-}$ and mineral species, show that the site has a history of highly acidic aerosol and is often influenced by periodically high concentrations of sea spray and crustal dust aerosol. Annually averaged sulfate concentrations measured at the SEARCH site have exceeded ammonium concentrations by 8 to 20 % over the continuous monitoring period 2008–2013 (see Fig. S10), showing that the high acidity calculated from data collected during the SOAS campaign is typical of this site. Furthermore, the two coarse particle events appear to have frequent precedents. Over the 5-year monitoring period, the site experienced 12–20 crustal dust events per year, and 20–42 sea spray events per year. Definitions of these events, annual totals, and full time series of mineral composition data are shown in the Supplement.

5 Conclusions

Gas and aerosol measurements of inorganic species in Centreville, AL, indicate the importance of crustal dust and sea spray in the region. The southeastern United States is characterized by high emissions of SO$_2$, leading to high concentrations of aerosol SO$_4^{2-}$, which available NH$_4^+$ is insufficient to balance, despite the high solubility of NH$_3$ in

acidic solutions. The acidic aerosol in this region also means HNO$_3$ is not readily soluble and the formation of fine-mode NH$_4$NO$_3$ is thermodynamically unfavorable. Instead, inorganic nitrate in the southeastern United States likely exists in the form of supermicron NO$_3^-$ balanced by the presence of mineral cations arising from transport of crustal dust and sea spray aerosol. Studies of aerosol composition and heterogeneous uptake rates of HNO$_3$ onto particle surfaces during the campaign indicate that NO$_3^-$ is formed predominantly from this pathway, with aerosol NO$_3^-$ formation likely limited by the availability of crustal dust surfaces. However, because coarse-mode NO$_3^-$ is under-measured, the actual contribution of this process to aerosol-phase NO$_3^-$ may be larger than in situ PM$_{2.5}$ measurements would suggest. Analysis of historical aerosol composition data collected at this site also shows acidity and crustal dust levels similar to those found during the summer 2013 SOAS campaign, indicating the long-term importance of acidity and crustal dust and the need for consideration of these factors during assessments of the chemistry of the atmosphere, particularly in the southeastern United States.

References

Arimoto, R., Ray, B. J., Lewis, N. F., Tomza, U., and Duce, R. A.: Mass-particle size distributions of atmospheric dust and the dry deposition of dust to the remote ocean, J. Geophys. Res.-Atmos., 102, 15867–15874, 1997.

Ault, A. P., Peters, T. M., Sawvel, E. J., Casuccio, G. S., Willis, R. D., Norris, G. A., and Grassian, V. H.: Single-particle SEM-EDX analysis of iron-containing coarse particulate matter in an urban environment: sources and distribution of iron within Cleveland, Ohio, Environ. Sci. Technol., 46, 4331–4339, 2012.

Ault, A. P., Guasco, T. L., Ryder, O. S., Baltrusaitis, J. Cuadra-Rodriguez, L. A., Collins, D. B., Ruppel, M. J., Bertram, T. H., Prather, K. A., and Grassian, V. H.: Inside versus outside: Ion redistribution in nitric acid reacted sea spray aerosol particles as determined by single-particle analysis, J. Am. Chem. Soc., 135, 14528–14531, 2013a.

Ault, A. P., Moffet, R. C., Baltrusaitis, J., Collins, D. B., Ruppel, M. J., Cuadra-Rodriguez, L. A., Zhao, D., Guasco, T. L., Ebben, C. J., Geiger, F. M., Bertram, T. H., Prather, K. A., and Grassian, V. H.: Size-dependent changes in sea spray aerosol composition and properties with different seawater conditions, Environ. Sci. Technol., 47, 5603–5612, 2013b.

Ayres, B. R., Allen, H. M., Draper, D. C., Brown, S. S., Wild, R. J., Jimenez, J. L., Day, D. A., Campuzano-Jost, P., Hu, W., de Gouw, J., Koss, A., Cohen, R. C., Duffey, K. C., Romer, P., Baumann, K., Edgerton, E., Takahama, S., Thornton, J. A., Lee, B. H., Lopez-Hilfiker, F. D., Mohr, C., Goldstein, A. H., Olson, K., and Fry, J. L.: Organic nitrate aerosol formation via NO_3 + BVOC in the Southeastern US, Atmos. Chem. Phys. Discuss., 15, 16235–16272, doi:10.5194/acpd-15-16235-2015, 2015.

Baker, K. and Scheff, P.: Photochemical model performance for PM2.5 sulfate, nitrate, ammonium, and precursor species SO_2, HNO_3, and NH_3 at background monitor locations in the central and eastern United States, Atmos. Environ., 41, 6185–6195, 2007.

Bauer, S. E., Koch, D., Unger, N., Metzger, S. M., Shindell, D. T., and Streets, D. G.: Nitrate aerosols today and in 2030: a global simulation including aerosols and tropospheric ozone, Atmos. Chem. Phys., 7, 5043–5059, doi:10.5194/acp-7-5043-2007, 2007.

Blanchard, C. and Hidy, G.: Effects of changes in sulfate, ammonia, and nitric acid on particulate nitrate concentrations in the southeastern United States, J. Air Waste Manage., 53, 283–290, 2003.

Blanchard, C. L., Roth, P. M., and Tanenbaum, S. J.: The use of ambient measurements to identify which precursor species limit aerosol nitrate formation, J. Air Waste Manage., 50, 2073–2084, 2000.

Bondy, A. L., Craig, R. L., Wang, B., Laskin, A., Nhliziyo, M. V., Bertman, S. B., Shepson, P. B., Pratt, K. A., and Ault, A. P.: Varying reactivity of sea spray aerosol transported inland in the southeastern United States, in preparation, 2015.

Brauer, M., Koutrakis, P., Keeler, G., and Spengler, J.: Indoor and outdoor concentrations of inorganic acidic aerosols and gases, J. Air Waste Manage., 42, 171–181, 1991.

Brimblecombe, P. and Clegg, S.: The solubility and behavior of acidic gases in the marine aerosol, J. Atmos. Chem., 7, 1–18, doi:10.1007/BF00048251, 1988.

Coz, E., Gómez-Moreno, F. J., Pujada, M., Casuccio, G. S., Lersch, T. L., and Artiñano, B.: Individual particle characteristics of North African dust under different long-range transport scenarios, Atmos. Environ., 43, 1850–1863, 2009.

Culkin, F. and Cox, R. A.: Sodium, potassium, magnesium, calcium, and strontium in sea water, Deep Sea Res. Ocean. Abstr., 13, 789–804, 1976.

Dentener, F. J., Carmichael, G. R., Zhang, Y., Lelieveld, J., and Crutzen, P. J.: Role of mineral aerosol as a reactive surface in the global troposphere, J. Geophys. Res.-Atmos., 101, 22869–22889, 1996.

Doering, O., Galloway, T., and Swackhamer, D.: Reactive Nitrogen in the United States: an analysis of inputs, flows, consequences, and management options, United States Environmental Protection Agency, 2011.

Durham, J. L. and Stockburger, L.: Nitric acid-air diffusion coefficient: Experimental determination, Atmos. Environ., 20, 559–563, 1967.

Edgerton, E., Hartsell, B., Saylor, R., Jansen, J., Hansen, D., and Hidy, G.: The Southeastern Aerosol Research and Characterization study: Part II. Filter-based measurements of fine and coarse particulate matter mass and composition, J. Air Waste Manage., 10, 1527–1542, 2005.

Edgerton, E., Casuccio, G., Saylor, R. D., Lersch, T. L., Hartsell, B. E., Jansen, J. J., and Hansen, D. A.: Measurements of OC and EC in coarse particulate matter in the southeastern United States, J. Geophys. Res.-Atmos., 59, 78–90, 2009.

Erickson, D. J. I., Seuzaret, C., Keene, W. C., and Gong, S. L.: A general circulation model based on calculation of HCl and $ClNO_2$ production from sea salt dechlorination: Reactive Chlorine Emissions Inventory, J. Geophys. Res.-Atmos., 104, 8347–8372, 1999.

Evans, M. C., Campbell, S. W., Bhethanabotla, V., and Poor, N. D.: Effect of sea salt and calcium carbonate interactions with nitric acid on the direct dry deposition of nitrogen to Tampa Bay, Florida, Atmos. Environ., 38, 4847–4858, 2004.

Finlayson-Pitts, B. J. and Pitts, J. N.: Chemistry of the Upper and Lower Atmosphere: Theory, Experiments, and Applications, Academic Press, San Diego, CA, 2000.

Fountoukis, C. and Nenes, A.: ISORROPIA II: a computationally efficient thermodynamic equilibrium model for K^+–Ca^{2+}–Mg^{2+}–NH_4^+–Na^+–SO_4^{2-}–NO_3^-–Cl^-–H_2O aerosols, Atmos. Chem. Phys., 7, 4639–4659, doi:10.5194/acp-7-4639-2007, 2007.

Fridlind, A. M. and Jacobson, M. Z.: A study of gas-aerosol equilibrium and aerosol pH in the remote marine boundary layer during the First Aerosol Characterization Experiment (ACE 1), J. Geophys. Res.-Atmos., 105, 17325–17340, 2000.

Fuchs, N. A. and Sutugin, A. G.: High dispersed aerosols, in: Topics in Current Aerosol Research (Part 2), edited by: Hidy, G. M. and Brock, J. R., Pergamon, New York, 2541–2548, 1971.

Gibson, E., Hudson, P., and Grassian, V.: Physicochemical properties of nitrate aerosols: implications for the atmosphere, J. Phys. Chem. A, 110, 11785–11799, 2006.

Goldstein, A., Koven, C., Heald, C., and Fung, I.: Biogenic carbon and anthropogenic pollutants combine to form a cooling haze over the southeastern United States, P. Natl. Acad. Sci. USA, 106, 8835–8840, 2009.

Guo, H., Xu, L., Bougiatioti, A., Cerully, K. M., Capps, S. L., Hite Jr., J. R., Carlton, A. G., Lee, S.-H., Bergin, M. H., Ng, N. L., Nenes, A., and Weber, R. J.: Fine-particle water and pH in the southeastern United States, Atmos. Chem. Phys., 15, 5211–5228, doi:10.5194/acp-15-5211-2015, 2015.

Hansen, D. A., Edgerton, E. S., Hartsell, B. E., Jansen, J. J., Kandasamy, N., Hidy, G. M., and Blanchard, C. L.: The Southern Aerosol Research and Characterization Study: Part 1 – Overview, J. Air Waste Manage., 53, 1460–1471, 2003.

Hennigan, C. J., Izumi, J., Sullivan, A. P., Weber, R. J., and Nenes, A.: A critical evaluation of proxy methods used to estimate the acidity of atmospheric particles, Atmos. Chem. Phys., 15, 2775–2790, doi:10.5194/acp-15-2775-2015, 2015.

Hopkins, R. J., Desyaterik, Y., Tivanski, A. V., Zaveri, R. A., Berkowitz, C. M., Tyliszczak, T., Gilles, M. K., and Laskin, A.: Chemical speciation of sulfur in marine cloud droplets and particles: Analysis of individual particles from the marine boundary layer over the California current, J. Geophys. Res.-Atmos., 113, D008954, doi:10.1029/2007JD008954, 2008.

Huffman, J. A., Sinha, B., Garland, R. M., Snee-Pollmann, A., Gunthe, S. S., Artaxo, P., Martin, S. T., Andreae, M. O., and Pöschl, U.: Size distributions and temporal variations of biological aerosol particles in the Amazon rainforest characterized by microscopy and real-time UV-APS fluorescence techniques during AMAZE-08, Atmos. Chem. Phys., 12, 11997–12019, doi:10.5194/acp-12-11997-2012, 2012.

Jacob, D. J.: Introduction to Atmospheric Chemistry, Princeton University Press, Princeton, NJ, 1999.

Jordan, C. E., Pszenny, A. A. P., Keene, W. C., Cooper, O. R., Deegan, B., Maben, J. R., Routhier, M., Sander, R., and Young, A. H.: Origins of aerosol chlorine during winter over north central Colorado, USA, J. Geophys. Res., 120, 678–694, 2015.

Kane, M. M., Rendell, A. R., and Jickells, T. D.: Atmospheric scavenging processes over the North Sea, Atmos. Environ., 28, 2523–2530, 1994.

Karydis, V. A., Tsimpidi, A. P., Fountoukis, C., Nenes, A., Zavala, M., Lei, W., Molina, L. T., and Pandis, S. N.: Simulating the fine and coarse inorganic particulate matter concentrations in a polluted megacity, Atmos. Environ., 44, 608–620, 1988.

Karydis, V. A., Tsimpidi, A. P., Pozzer, A., Astitha, M., and Lelieveld, J.: Effects of mineral dust on global atmospheric nitrate concentrations, Atmos. Chem. Phys. Discuss., 15, 11525–11572, doi:10.5194/acpd-15-11525-2015, 2015.

Keuken, M. P., Schoonebeek, C. A. M., van Wensveen-Louter, A., and Slanina, J.: Simultaneous sampling of NH$_3$, HNO$_3$, HCl, SO$_2$ and H$_2$O$_2$ in ambient air by a wet annular denuder system, Atmos. Environ., 22, 2541–2548, 1988.

Khlystov, A., Stanier, C., and Pandis, S. N.: An algorithm for combining electrical mobility and aerodynamic size distributions data when measuring ambient aerosol, Aerosol Sci. Technol., 38, 229–238, 2004.

Koutrakis, P., Wolfson, J., and Spengler, J.: An improved method for measuring aerosol strong acidity: results from a nine-month study in St. Louis, Missouri and Kingston, Tennessee, Atmos. Environ., 22, 157–162, 1988.

Krueger, B. J., Grassian, V. H., Cowin, J. P., and Laskin, A.: Heterogeneous chemistry of individual mineral dust particles from different dust source regions: the importance of particle mineralogy, Atmos. Environ., 38, 6253–6261, 2004.

Kulkarni, S.: Calibration and check samples for ED-XRF and WD-XRF, KulTech Incorporated, 311 S. Academy Street, Cary, NC 27511, brochure, 2010.

Laskin, A., Idedema, M. J., and Cowin, J. P.: Quantitative time-resolved monitoring of nitrate formation in sea salt particles using a CCSEM/EDX single particle analysis, Environ. Sci. Technol., 36, 4948–4955, 2002.

Laskin, A., Iedema, M. J., Ichkovich, A., Graber, E. R., Taraniuk, I., and Rudich, Y.: Direct observation of completely processed calcium carbonate dust particles, Faraday Discuss., 130, 453–468, 2005a.

Laskin, A., Wietsma, T. W., Krueger, B. J., and Grassian, V. H.: Heterogeneous chemistry of individual mineral dust particles with nitric acid: A combined CCSEM/EDX, ESEM, and ICP-MS study, J. Geophys. Res.-Atmos., 110, D10208, doi:10.1029/2004JD005206, 2005b.

Laskin, A., Cowin, J. P., and Iedema, M. J.: Analysis of individual environmental particles using modern methods of electron microscopy and X-ray microanalysis, J. Electron Spectrosc., 150, 260–274, 2006.

Laskin, A., Moffet, R. C., Gilles, M. K., Fast, J. D., Zaveri, R. A., Wang, B. B., Nigge, P., and Shutthanandan, J.: Tropospheric chemistry of internally mixed sea salt and organic particles: Surprising reactivity of NaCl with weak organic acids, J. Geophys. Res.-Atmos., 117, D017743, doi:10.1029/2012JD017743, 2012.

Lee, T., Yu, X., Ayres, B., Kreidenweis, S. M., Malm, W. C., and Collett, J. L.: Observations of fine and coarse particle nitrate at several rural locations in the United States, Atmos. Environ., 42, 2720–2732, 2008.

Li, J., Posfai, M., Hobbs, P. V., and Buseck, P. R.: Individual aerosol particles from biomass burning in southern Africa: 2. Compositions and aging of inorganic particles, J. Geophys. Res.-Atmos., 108, 8484, doi:10.1029/2002JD002310, 2003.

Liu, Y., Cain, J. P., Wang, H., and Laskin, A.: Kinetic study of heterogeneous reaction of deliquesced NaCl particles with gaseous HNO$_3$ using particle-on-substrate stagnation flow reactor approach, J. Phys. Chem. A, 111, 10026–10042, 2007.

Makkonen, U., Virkkula, A., Mäntykenttä, J., Hakola, H., Keronen, P., Vakkari, V., and Aalto, P. P.: Semi-continuous gas and inorganic aerosol measurements at a Finnish urban site: comparisons with filters, nitrogen in aerosol and gas phases, and aerosol acidity, Atmos. Chem. Phys., 12, 5617–5631, doi:10.5194/acp-12-5617-2012, 2012.

Markovic, M. Z., Hayden, K. L., Murphy, J. G., Makar, P. A., Ellis, R. A., Chang, R. Y.-W., Slowik, J. G., Mihele, C., and Brook, J.: The effect of meteorological and chemical factors on the agreement between observations and predictions of fine aerosol composition in southwestern Ontario during BAQS-Met,

Atmos. Chem. Phys., 11, 3195–3210, doi:10.5194/acp-11-3195-2011, 2011.

Meng, Z. and Seinfeld, J. H.: Time scales to achieve atmospheric gas-aerosol equilibrium for volatile species, Atmos. Environ., 30, 2889–2900, 1996.

Metzger, S., Mihalopoulos, N., and Lelieveld, J.: Importance of mineral cations and organics in gas-aerosol partitioning of reactive nitrogen compounds: case study based on MINOS results, Atmos. Chem. Phys., 6, 2549–2567, doi:10.5194/acp-6-2549-2006, 2006.

Moffet, R. C., Henn, T. R., Tivanski, A. V., Hopkins, R. J., Desyaterik, Y., Kilcoyne, A. L. D., Tyliszczak, T., Fast, J., Barnard, J., Shutthanandan, V., Cliff, S. S., Perry, K. D., Laskin, A., and Gilles, M. K.: Microscopic characterization of carbonaceous aerosol particle aging in the outflow from Mexico City, Atmos. Chem. Phys., 10, 961–976, doi:10.5194/acp-10-961-2010, 2010.

Moffet, R. C., Rödel, T. C., Kelly, S. T., Yu, X. Y., Carroll, G. T., Fast, J., Zaveri, R. A., Laskin, A., and Gilles, M. K.: Spectro-microscopic measurements of carbonaceous aerosol aging in Central California, Atmos. Chem. Phys., 13, 10445–10459, doi:10.5194/acp-13-10445-2013, 2013.

Pilson, M. E. Q.: An Introduction to the Chemistry of the Sea, Prentice Hall, New York, 1998.

Portmann, R., Solomon, S., and Hegerl, G.: Spatial and season patterns in climate change, temperatures, and precipitation across the United States, P. Natl. Acad. Sci. USA, 106, 7324–7329, 2009.

Posfai, M., Simonics, R., Li, J., Hobbs, P. V., and Buseck, P. R.: Individual aerosol particles from biomass burning in southern Africa: 1. Compositions and size distributions of carbonaceous particles, J. Geophys. Res.-Atmos., 108, 8483, doi:10.1029/2002JD002291, 2003.

Rumsey, I. C., Cowen, K. A., Walker, J. T., Kelly, T. J., Hanft, E. A., Mishoe, K., Rogers, C., Proost, R., Beachley, G. M., Lear, G., Frelink, T., and Otjes, R. P.: An assessment of the performance of the Monitor for AeRosols and GAses in ambient air (MARGA): a semi-continuous method for soluble compounds, Atmos. Chem. Phys., 14, 5639–5658, doi:10.5194/acp-14-5639-2014, 2014.

Russell, A. R., Valin, L. C., and Cohen, R. C.: Trends in OMI NO_2 observations over the United States: effects of emission control technology and the economic recession, Atmos. Chem. Phys., 12, 12197–12209, doi:10.5194/acp-12-12197-2012, 2012.

Sander, S. P., Abbatt, J., Barker, J. R., Burkholder, J. B., Friedl, R. R., Golden, D. M., Huie, R. E., Kolb, C. E., Kurylo, M. J., Moortgat, G. K., Orkin, V. L., and Wine, P. H.: Chemical kinetics and photochemical data for use in atmospheric studies, evaluation No. 17, JPL publication 10-6, Jet Propulsion Laboratory, Pasadena, available at: http://jpldataeval.jpl.nasa.gov/ (last access: 20 August 2015), 2011.

Saxena, P., Mueller, P. K., Kim, Y. P., Seinfeld, J. H., and Koutrakis, P.: Coupling thermodynamic theory with measurements to characterize acidity of atmospheric particles, Aerosol Sci. Technol., 19, 279–293, 1993.

Seinfeld, J. H. and Pandis, S. N.: Atmospheric Chemistry and Physics: From Air Pollution to Climate Change, John Wiley & Sons, New York, 2nd Edn., 2006.

Slanina, J., ten Brink, H., Otjes, R., Even, A., Jongejan, P., Khlystov, A., Waijers-Ijpelaan, A., Hu, M., and Lu, Y.: The continuous analysis of nitrate and ammonium in aerosols by the steam jet aerosol collector (SJAC): extension and validation of the methodology, Atmos. Environ., 35, 2319–2330, 2001.

Sobanska, S., Coeur, C., Maenhaut, W., and Adams, F.: SEM-EDX characterization of tropospheric aerosols in the Nagev desert (Israel), J. Atmos. Chem., 44, 299–322, 2003.

Spengler, J., Keeler, G., Koutrakis, P., Ryan, P., Raisenne, M., and Franklin, C.: Exposures to acidic aerosol, Environ. Health Persp., 79, 43–51, 1989.

Stelson, A. W. and Seinfeld, J. H.: Thermodynamic prediction of the water activity, NH_4NO_3 dissociation constant, density and refractive index for the NH_4NO_3-$(NH_4)_2SO_4$-H_2O system at 25 °C, Atmos. Environ., 16, 2507–2514, 1982.

Stohl, A., Hittenberger, M., and Wotawa, G.: Validation of the Lagrangian particle dispersion model FLEXPART against large-scale tracer experiment data, Atmos. Environ., 32, 4245–4264, 1998.

Stohl, A., Eckhardt, S., Forster, C., James, P., Spichtinger, N., and Seibert, P.: A replacement for simple back trajectory calculations in the interpretation of atmospheric trace substance measurements, Atmos. Environ., 36, 4635–4648, 2002.

Trebs, I., Meixner, F. X., Slanina, J., Otjes, R., Jongejan, P., and Andreae, M. O.: Real-time measurements of ammonia, acidic trace gases and water-soluble inorganic aerosol species at a rural site in the Amazon Basin, Atmos. Chem. Phys., 4, 967–987, doi:10.5194/acp-4-967-2004, 2004.

Trebs, I., Metzger, S., Meixner, F. X., Helas, G., Hoffer, A., Rudich, Y., Falkovich, A., Moura, M. A. L., da Silva, R. S., Artaxo, P., Slanina, J., and Andreae, M. O.: The NH_4^+-NO_3^--Cl^--SO_4^{2-}-H_2O aerosol system and its gas phase precursors at a pasture site in the Amazon Basin: How relevant are mineral cations and soluble organic acids?, J. Geophys. Res.-Atmos., 110, D07303, doi:10.1029/2004JD005478, 2005.

Underwood, G., Song, C., Phadnis, M., Carmichael, G., and Grassian, V.: Heterogeneous reactions of NO_2 and HNO_3 on oxides and mineral dust: A combined laboratory and modeling study, J. Geophys. Res.-Atmos., 106, 18055–18066, 2001.

Usher, C., Michel, A., and Grassian, V.: Reactions on mineral dust, Chem. Rev., 103, 4883–4939, 2003.

Utsunomiya, S., Jenson, K. A., Keeler, G. J., and Ewing, R. C.: Direct identification of trace metals in fine and ultrafine particles in the Detroit urban atmosphere, Environ. Sci. Technol., 38, 2289–2297, 2004.

von der Weiden, S.-L., Drewnick, F., and Borrmann, S.: Particle Loss Calculator – a new software tool for the assessment of the performance of aerosol inlet systems, Atmos. Meas. Tech., 2, 479–494, doi:10.5194/amt-2-479-2009, 2009.

Wang, B. and Laskin, A.: Reactions between water-soluble organic acids and nitrates in atmospheric aerosols: recycling of nitric acid and formation of organic salts, J. Geophys. Res.-Atmos., 119, 3335–3351, 2014.

Wexler, A. and Clegg, S.: Atmospheric aerosol models for systems including the ions H^+, NH_4^+, Na^+, SO_4^{2-}, NO_3^-, Cl^-, Br^-, and H_2O, J. Geophys. Res.-Atmos., 107, 4207, doi:10.1029/2001JD000451, 2007.

Yeatman, S., Spokes, L., and Jickells, T.: Comparisons of coarse-mode aerosol nitrate and ammonium at two polluted coastal sites, Atmos. Environ., 35, 1321–1335, 2001.

Young, A. H., Keene, W. C., Pszenny, A. P., Sander, R., Thornton, J. A., Riedel, T. P., and Maben, J. R.: Phase partitioning of soluble trace gases with size-resolved aerosols in near-surface continental air over northern Colorado, USA, during winter, J. Geophys. Res.-Atmos., 118, 9414–9427, 2013.

Zhuang, H., Chan, C. K., Fang, M., and Wexler, A. S.: Formation of nitrate and non-sea-salt sulfate on coarse particles, Atmos. Environ., 33, 4223–4233, 1999.